Efficient prediction of aerodynamic interference in multirotor systems

Furkat Yunus[1] Assistant Professor
Gianluca Romani[2] Software Engineering Manager
Damiano Casalino[2] R&D Technology Director
Marilena Pavel[1] Associate Professor
Mirjam Snellen[1] Full Professor

[1] Control and Operations Department, Faculty of Aerospace Engineering, Delft University of Technology, Delft, The Netherlands
[2] SIMULIA Fluids R&D, Dassault Systemes Deutschland GmbH, Stuttgart, Germany

ABSTRACT

This paper introduces a computationally efficient method for predicting aerodynamic interference effects in multirotor systems during forward flight. The approach combines a finite-state dynamic inflow model with both analytical and prescribed wake models. To assess its accuracy and performance, the method is validated against high-fidelity CFD simulations for a twin-rotor configuration. Results show that the proposed model effectively captures rotor-rotor aerodynamic interactions, making it well-suited for rapid preliminary evaluations of aerodynamic and aeroacoustic performance in multirotor designs.

INTRODUCTION

Urban Air Mobility (UAM) has attracted significant global interest in recent years. To meet future market demands, both startups and established aircraft OEMs are developing novel electric vertical take-off and landing (eVTOL) aircraft for intercity travel. However, several engineering challenges must be addressed before eVTOLs become viable, particularly in designing low-noise propulsion systems. The multirotor configuration of these aircraft introduces complex aerodynamic interactions that contribute to noise generation, an aspect often overlooked in early-stage design exploration. Depending on rotor arrangement, these interactions can either enhance or degrade performance while significantly influencing noise radiation (Ref. Zawodny et al., 2023). The aerodynamic interaction among rotors can be a significant source compared to the isolated rotor noise, especially for applications with limited tip Mach numbers, such as typical UAM vehicles (Ref. Zarri et al., 2022). Furthermore, properly accounting for the acoustic features induced by these interactions could be valuable for psycho-acoustic annoyance studies. The goal of the present paper is to focus on the aerodynamic interference between the rotors, presenting an efficient computational approach that can be used during design and trajectory optimization applications. A detailed analysis of the resulting noise emissions, however, is beyond the scope of this work and will be addressed in future studies.

Analytical methods based on simple vortex theory have been explored to efficiently model rotor interference. Luo et al. (Ref. Luo et al., 2015) proposed a simplified approach by combining momentum theory with interference factors from (Ref. Johnson, 2012), focusing on mutual interference in a "+"-shaped quadrotor. They modeled rotor interaction analogously to fixed-wing formation flight, treating a spinning rotor in forward flight as a circular wing that generates and rolls up wake structures (Ref. Ghee et al., 1996). The rolled-up wake, referred to as apparent disc or edge vortices (Refs. Roos, 1996, Yunus et al., 2025b), was considered as the primary mechanism of rotor-rotor interference. Their model, validated against CFD results, showed good correlation but is limited to "+"-configured quadrotors and relies on simplifying assumptions. It does not account for wake roll-up on advancing and retreating sides or the lateral and axial positions of vortices, making it less comprehensive. Nguyen et al. (Ref. Nguyen et al., 2018) developed an analytical approach combining momentum theory and a simplified horseshoe vortex to model interference in a multirotor system. While the model's results were consistent with experimental data, the authors noted that the primary source of discrepancy stemmed from the simplifications in the horseshoe vortex model. Han and Barakos (Ref. Han and Barakos, 2020) proposed a simplified formulation to address the interference of arbitrarily configured multirotor systems. The model uses a simplified horseshoe vortex derived from a circular wing approximation (Ref. Leishman, 2006), which is valid only when the rotor's advance ratio exceeds 0.1. Additionally, the results from this formulation showed significant discrepancies in terms of clearance betweeen rotors (Ref. Nguyen et al., 2018). Guner and Prasad (Refs. Guner and Prasad, 2022, Güner, 2022) improved upon the simple horseshoe vortex model by using an azimuthal vorticity distribution derived from Heyson (Ref. Heyson, 1960). They studied the effects of rotor overlap on induced power in multirotor systems, validating their approach across configurations such as coaxial and tandem rotors, with good agreement to experimental data and high-fidelity analyses. While effective for preliminary multirotor design, the model has limitations, particularly in accurately capturing interference effects for non-overlapping rotors (at hub-to-hub separations d > 2R). Additionally, momentum theory overlooks the rotation direction, which is crucial for balancing net torque in multirotor systems. To address this limitation, Usov et al. (Ref. Usov et al., 2022) developed a reduced-order model based on combined inflow theory to predict aerodynamic interference between non-overlapping rotors. They replaced simple vortex theory with Beddoes's generalized wake model and substituted momentum theory with the finite-state inflow model by Peters and He (Ref. Peters and He, 1995). This improved the resolution of aerodynamic loads by capturing the spatially varying induced inflow across the rotor disk, rather than assuming uniform inflow at the hub. However, a key limitation is that only tip vortices—as prescribed by the Beddoes model—were included, neglecting disk-edge vortices and their contribution to rotor-rotor aerodynamic interference. Moreover, the method remains computationally intensive, highlighting the need for further efficiency improvements.

The authors developed a computational approach coupling the Peters–He finite-state dynamic inflow model with both an analytical and a prescribed wake model to predict the lateral and axial positions of roll-up and tip vortices during forward flight (Ref. Yunus et al., 2025b). The analytical wake model, originally formulated for helicopter rotors, is extended here to capture disc-edge vortex position and geometry at advance ratios above 0.15. The prescribed wake model employs the Beddoes formulation. Building on this foundation, the present study applies this combined framework to predict aerodynamic interference in multirotor systems during forward flight. This represents a novel integration of established models and their validation against high-fidelity CFD simulations—constituting the study's primary contribution. Although the focus here is on rotor-rotor interference in a tandem configuration, the methodology is readily extendable to multirotor systems with arbitrary blade counts and rotation directions.

METHODOLOGY

A hybrid approach is used to predict aerodynamic interference between rotors. Each rotor's self-induced inflow is computed via the Peters–He finite-state inflow model (Ref. Peters and He, 1995). The interference-induced inflow from disc-edge vortices is predicted using the authors' analytical wake model (Ref. Yunus et al., 2025b), while the interference due to trailed tip vortices is modeled with the Beddoes prescribed wake formulation. The total induced velocity at each rotor is then obtained by superposing its self-induced inflow with the interference-induced inflows from all other rotors.

Self-Induced Velocity Model

The self-induced velocity field $\lambda_i(\bar{r}, \psi, t)$ on the rotor disk is computed using the Peters–He finite-state inflow model (Ref. Peters and He, 1995), which provides a nondimensional representation of the induced velocity. A detailed exposition of the model's theoretical background and development can be found in (Refs. Peters and He, 1995, Moriarty and Hansen, 2005, Li, 2020).

In the Peters–He model the normal component of induced velocity on the rotor disk is expressed as a double-infinite series expansion comprising azimuthal Fourier harmonics and radial Legendre functions. Truncating this infinite series to a finite number of terms yields a finite set of inflow states that describe the induced velocity distribution across the rotor disk. Specifically, the induced velocity is approximated by truncating the series to m Fourier harmonics in the azimuthal direction and n Legendre functions in the radial direction, resulting in an $m \times n$ dynamic inflow model. The parameters m and n are user-defined and should be chosen to balance accuracy with computational efficiency, which is critical in design applications. Typically, m is related to the blade count N_b. For instance, in (Ref. Usov et al., 2022), m was set equal to N_b, sufficient for steady-state predictions, while n (denoted p in their work) was set to 4 to ensure aerodynamic load convergence. Conversely, (Ref. Ho and Yeo, 2021) sets both m and n to $3N_b$ to achieve a favorable trade-off between accuracy and computational speed. Unless otherwise specified, all calculations in this paper use 90 azimuthal steps per revolution.

Interference Induced Velocity Model

The interference-induced velocity from rolled-up disk edge vortices, $w_{\mathrm{D}i}(\bar{r}, \psi, t)$, is computed using the analytical wake model developed by the authors (Ref. Yunus et al., 2025b), which predicts the location, geometry, and strength of these vortices. In contrast, the interference due to trailed tip vortices, $w_{\mathrm{T}i}(\bar{r}, \psi, t)$, is evaluated using the Beddoes prescribed wake model. Both models are implemented in LOPNOR-ARDYN and validated against high-fidelity CFD simulations (Ref. Yunus et al., 2025b). Tip vortex trajectories are updated at each time step based on blade azimuthal positions, whereas disk edge vortex trajectories are computed after loading convergence, as the analytical model represents time-averaged behavior (Ref. Roos, 1996). For both wake models, the vortex strength at a given azimuthal location is derived from the blade's maximum circulation. Once the vortex circulations are known, the induced velocity field is calculated using the Biot–Savart law. Full implementation details are available in the companion paper (Ref. Yunus et al., 2025b).

The dynamic inflow model depends on the flow conditions at the rotor disk. At the first time step, a blade element momentum theory (BEMT) solution—implemented in LOPNOR-BEMT (Refs. Yunus et al., 2025a, Yunus et al., 2024)—is used to compute the initial loading and inflow distributions, providing inputs for calculating self-induced inflow via the Peters–He model. Subsequently, the interference-induced velocities $w_{Di}(\bar{r},\psi,t)$ and $w_{Ti}(\bar{r},\psi,t)$ are computed using the Biot–Savart law and added to the self-induced inflow $\lambda_i(\bar{r},\psi,t)$ to define the total induced velocity field. For rotors operating in the wake of others, the azimuthally averaged interference-induced velocities are also added to the freestream inflow. This procedure is iterated until convergence of the inflow state is achieved.

GEOMETRY AND NUMERICAL SETUP

The geometry used in this study is a two-bladed propeller designed at TUDelft, and characterized by a radius R = 0.15 m and NACA 4412 airfoil sections. Additional details about the employed geometry can be found in (Ref. Casalino et al., 2021). This propeller has been extensively examined in previous experimental works (Refs. Grande et al., 2022b, Grande et al., 2022a). In the present work, high-fidelity (H-F) CFD simulations, using the commercial software SIMULIA PowerFLOW based on the Lattice-Boltzmann/Very Large Eddy Simulation (LB/VLES) method, have been carried out to generate reference data for validating the analytical model. The computational setup has been successfully validated in the past on the same propeller geometry in several numerical studies (Refs. Romani et al., 2022, Casalino et al., 2022, Casalino et al., 2023), where the interested reader can also find additional information about the LB/VLES flow solver. In the current work, a twin propeller in tandem configuration operated at 4000 RPM under edgewise flow conditions is considered, with a flow incidence angle $\alpha_d = 5°$ and a free-stream velocity $V = 10$ m/s, as sketched in Fig. 1. The hub-to-hub distance between the two propeller is set to three times the propeller radius. The two propeller rotate in opposite direction.

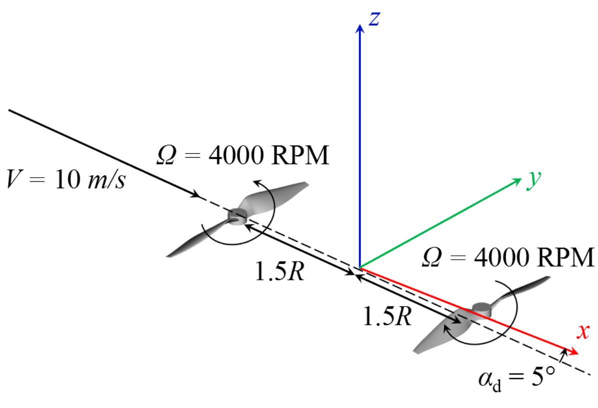

Figure 1: Propellers configuration and operating conditions.

The computational domain is a spherical volume of radius 120R centered around the hub-to-hub mid-point distance, i.e. (0, 0, 0) m. Free-stream static pressure (101325 Pa) and velocity (10 m/s), and turbulence intensity of 0.1% of the freestream velocity are prescribed on its outer boundary. Figure 2 shows the details of the computational grid and setup. Each propeller and hub couple is encompassed by a volume of revolution that defines the Local Reference Frame (LRF), i.e. the rotating sliding mesh domain used to reproduce the propeller rotation.

The LB/VLES scheme is solved on a Cartesian mesh composed of cubic volume elements (voxels) distributed within different Variable Resolution (VR) regions. A grid resolution change by a factor of two characterizes adjacent VRs. A total of 14 VR regions are used to discretize the whole fluid domain, with the finest resolution level (VR13) placed around the blade. A resolution of 100 voxels along the mean chord (22.85 mm) is used within this finest resolution level, resulting in a smallest voxel size of 0.022 mm, a mean $y^+ \simeq 5$ on the blade surface. The second finest VR is applied on the whole propeller geometry and in the near tip vortex region, while the third finest level (VR11) is used to finely discretize the propeller wake region, thus allowing the comparison with the analytical models for a sufficient number of wake spirals. All the other VRs consist of boxes or spheres that are used to discretize the rest of the fluid domian up to its boundaries. The overall mesh consists of 188 million voxels and 41.4 million fine-equivalent voxels. The whole fluid domain is initialized with the instantaneous flow solution from a statistically converged coarser simulation. Hence, after a settling time corresponding to 2 propeller revolutions, the sampling of relevant flow data is started for 2 additional revolutions.

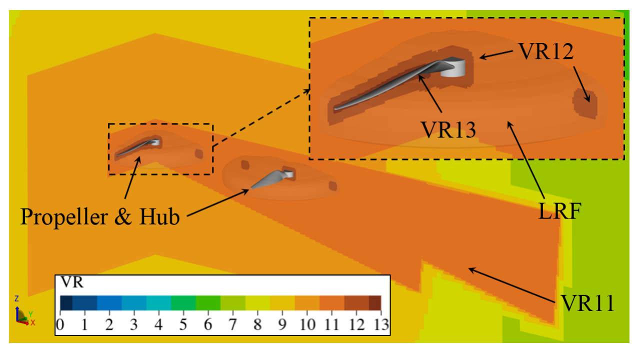

Figure 2: Details of the computational setup and grid.

RESULTS

The mean-removed sectional thrust distribution over the rotor disk computed using LOPNOR-ARDYN is compared against high-fidelity (H-F) CFD simulation results in Fig.3. The results show that the front rotor's thrust distribution closely matches that of the isolated rotor, indicating that the aerodynamic interference from the aft rotor has negligible effect on the front rotor in this configuration. In contrast, the aft rotor experiences a substantial impact from the wake of the front rotor, leading to a notable alteration in its thrust distribution. This asymmetric interaction is consistent with findings from (Refs. Misiorowski et al., 2019, Healy et al., 2022), and reinforces the observation that rotor–rotor interaction predominantly affects the downstream rotor.

On the aft rotor, a localized thrust increase is observed near $\psi = 270°$, attributed to the upwash generated by the retreating side edge vortex of the front rotor—an effect also reported in (Ref. Healy et al., 2022). Interestingly, the H-F CFD results indicate that the aft rotor generates slightly more thrust than in the isolated case, while the front rotor remains unaffected. This behavior is counterintuitive, as aerodynamic interference typically leads to an increased inflow ratio on the aft rotor, which would normally result in reduced thrust and increased power consumption (Ref. Usov et al., 2022). The observed inverse trend is currently under further investigation.

The prediction of $\Delta CT_{\partial r}$ over the rotor disk from LOPNOR-ARDYN captures the overall trend of its variation well. However, it fails to accurately predict the maximum $\Delta CT_{\partial r}$ near $\psi = 270°$ on the aft rotor. This discrepancy is attributed to the reduced-order nature of the interference model implemented in LOPNOR-ARDYN and the specific modeling parameters chosen for this study. A parametric and sensitivity analysis will be conducted in future work to assess potential improvements in predictive accuracy. Further comparison between LOPNOR-ARDYN predictions and high-fidelity (H-F) CFD simulation results is presented in Fig. 4 at three radial stations: $r/R = 0.5$, $r/R = 0.7$, and $r/R = 0.9$. For simplicity, the aft rotor results are mapped onto the azimuth angle of the front rotor, allowing both to show peak values around $\psi = 90°$ and minima near $\psi = 270°$. At $r/R = 0.9$, distinct impulses appear on the advancing side of the disk, these are caused by blade–vortex interactions and are typical for edgewise rotors operating at transitional advance ratios (approximately 0.1–0.15) (Ref. Ho and Yeo, 2021). These impulses extend inboard to $r/R = 0.7$, although with diminished strength. Further inboard at $r/R = 0.5$, where the influence of tip vortices is minimal, the distribution exhibits a dominant 1/rev behavior, and both rotors display nearly identical trends. As a result, LOPNOR-ARDYN shows very good agreement with H-F CFD results at $r/R = 0.5$, favorable agreement at $r/R = 0.7$, and reasonable trend capture at $r/R = 0.9$, albeit with a noticeable underprediction of the peak thrust. This underprediction near the blade tip is expected due to the absence of a blade–wake interaction model (Ref. Ho and Yeo, 2021), and will be further investigated in future work by integrating such a model.

Accurate prediction of both rolled-up disk edge vortices and trailed tip vortices is essential for calculating the interference-induced velocity using the Biot–Savart law. Figure 5 presents a comparison of the axial locations of the disk edge and trailed tip vortices against high-fidelity (H-F) CFD simulation results. The model demonstrates good agreement with the H-F CFD data for the front rotor, successfully capturing both the disk edge and trailed tip vortex trajectories. However, for the aft rotor, the model underpredicts the deflection of the disk edge vortices, likely due to the strong downwash experienced by the aft rotor disk. In contrast, the trailed tip vortex trajectories of the aft rotor align reasonably well with the CFD results, capturing the general trend.

Overall, LOPNOR-ARDYN shows favorable agreement with the H-F CFD data, reinforcing its credibility in modeling rotor–rotor aerodynamic interactions.

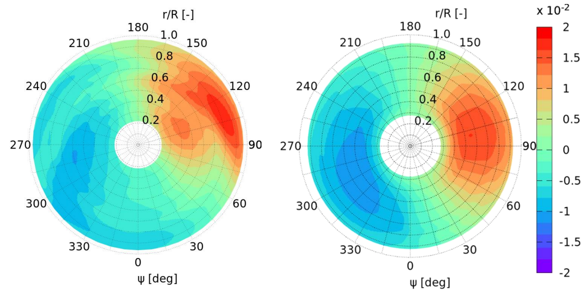

(a) H-F CFD simulation (left), LOPNOR-ARDYN (right).

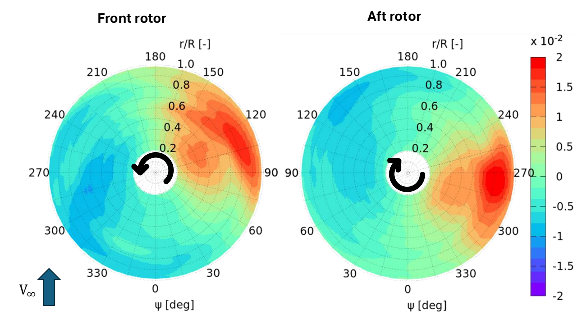

(b) H-F CFD simulation.

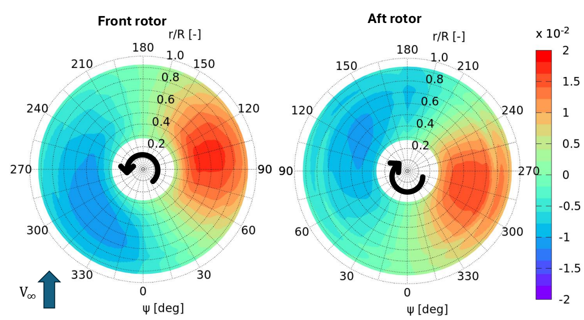

(c) LOPNOR-ARDYN.

Figure 3: Comparison of mean-removed sectional thrust coefficient distribution $\Delta CT_{\partial r}$ over the rotor disk: (a) isolated rotor, (b) tandem rotor—H-F CFD simulation, and (c) tandem rotor—LOPNOR-ARDYN prediction.

CONCLUSION

This work presents a computationally efficient approach for predicting aerodynamic interference effects in multi-rotor systems during forward flight. The self-induced velocity field is computed using the Peters–He dynamic inflow model, while the interference-induced velocity due to disk-edge vortices on both the retreating and advancing sides is calculated using an analytical model. The contribution from trailed tip vortices is evaluated using the Beddoes prescribed wake model.

High-fidelity CFD simulations using the commercial software SIMULIA PowerFLOW are performed for a tandem rotor configuration to validate the proposed approach. Results show that the front rotor experiences negligible aerodynamic interference and behaves similarly to an isolated rotor, indicating that the presence of the aft rotor has little to no effect on it. This trend is accurately captured by the proposed model.

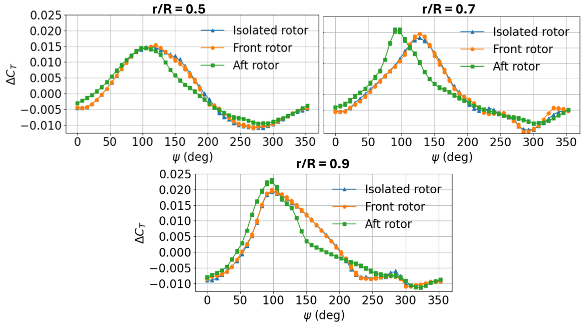

(a) H-F CFD simulation comparison against isolated rotor.

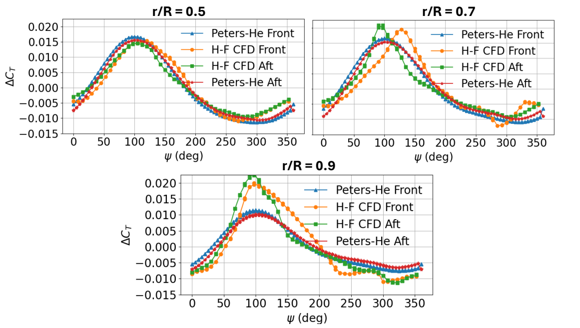

(b) Peters-He model comparison gainst H-F CFD simulation.

Figure 4: Comparison of the differential thrust coefficient distribution, $\Delta CT_{\partial r}$, between the front and aft rotors and an isolated rotor at three radial positions: $r/R = 0.5$, $r/R = 0.7$, and $r/R = 0.9$. (a) Results from high-fidelity (H-F) CFD simulations. (b) Predictions from LOPNOR-ARDYN .

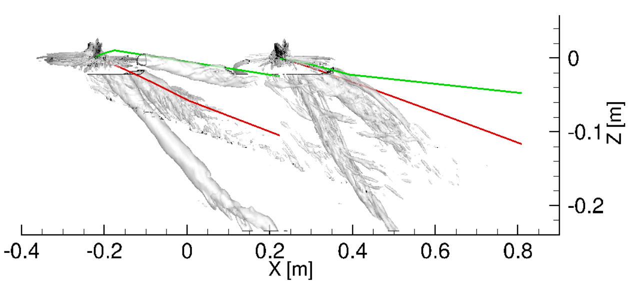

(a) Disc edge vortices axial locations.

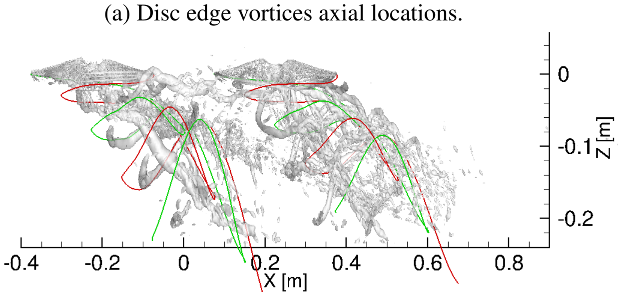

(b) Tip vortices axial locations.

Figure 5: Comparison of the axial locations of edge vortices calculated using the analytical wake model and the trailed tip vortex trajectories predicted by the Beddoes prescribed wake model against high-fidelity (H-F) CFD simulation data.

However, the model does not reproduce the increase in thrust observed around $\psi = 270°$ on the aft rotor, which is mainly concentrated near the tips of the blades.

The model successfully predicts the axial positions of disk-edge vortices on both the advancing and retreating sides of the front rotor. However, it underpredicts the deflection of the disk-edge vortices on the aft rotor, which are more strongly deflected downward due to the intensified downwash. In contrast, the predicted trailed tip vortex trajectories for both the front and aft rotors show favorable agreement with the CFD simulation results.

Overall, the results demonstrate favorable agreement with high-fidelity CFD data, providing reasonably accurate predictions of rotor disk loading as well as the locations of edge and tip vortices. The proposed model effectively captures rotor–rotor aerodynamic interactions, making it well-suited for rapid, preliminary evaluations of aerodynamic and aeroacoustic performance in multi-rotor configurations. This approach offers a valuable tool for future applications such as rotor–rotor interference modeling, multirotor noise prediction, and noise-optimal trajectory optimization for eVTOL operations in future air mobility systems.

REFERENCES

Casalino et al., 2021. Casalino, D., Grande, E., Romani, G., Ragni, D., and Avallone, F. (2021). Definition of a benchmark for low reynolds number propeller aeroacoustics. *Aerospace Science and Technology*, 113:106707.

Casalino et al., 2023. Casalino, D., Romani, G., Pii, L. M., and Colombo, R. (2023). Flow confinement effects on sUAS rotor noise. *Aerospace Science and Technology*, 143:108756.

Casalino et al., 2022. Casalino, D., Romani, G., Zhang, R., and Chen, H. (2022). Lattice-Boltzmann calculations of rotor aeroacoustics in transitional boundary layer regime. *Aerospace Science and Technology*, 130:107953.

Ghee et al., 1996. Ghee, T. A., Berry, J. D., Zori, L. A., and Elliott, J. W. (1996). Wake geometry measurements and analytical calculations on a small-scale rotor model. Technical report.

Grande et al., 2022a. Grande, E., Ragni, D., Avallone, F., and Casalino, D. (2022a). Laminar separation bubble noise on a propeller operating at low Reynolds numbers. *AIAA Journal*, 60(9):5324–5335.

Grande et al., 2022b. Grande, E., Romani, G., Ragni, D., Avallone, F., and Casalino, D. (2022b). Aeroacoustic investigation of a propeller operating at low Reynolds numbers. *AIAA Journal*, 60(2):860–871.

Güner, 2022. Güner, F. (2022). A multirotor inflow model based on combined momentum theory and simple vortex theory (cmtsvt) for flight simulations. In *78th Vertical Flight Society Annual Forum and Technology Display, FORUM 2022*.

Guner and Prasad, 2022. Guner, F. and Prasad, J. (2022). Combined momentum theory and simple vortex theory inflow model for multirotor configurations. *Journal of the American Helicopter Society*, 67(2):1–15.

Han and Barakos, 2020. Han, D. and Barakos, G. N. (2020). Aerodynamic interference model for multirotors in forward flight. *Journal of Aircraft*, 57(6):1220–1223.

Healy et al., 2022. Healy, R., Misiorowski, M., and Gandhi, F. (2022). A cfd-based examination of rotor-rotor separation effects on interactional aerodynamics for evtol aircraft. *Journal of the American Helicopter Society*, 67(1):1–12.

Heyson, 1960. Heyson, H. H. (1960). *Equations for the Induced Velocities Near a Lifitng Rotor with Nonuniform Azimuthwise Vorticity Distribution*. National Aeronautics and Space Administration.

Ho and Yeo, 2021. Ho, J. C. and Yeo, H. (2021). Evaluation of finite-state dynamic inflow for rotors. *Journal of Aircraft*, 58(5):1068–1082.

Johnson, 2012. Johnson, W. (2012). *Helicopter theory*. Courier Corporation.

Leishman, 2006. Leishman, G. J. (2006). *Principles of helicopter aerodynamics*. Cambridge university press.

Li, 2020. Li, S. (2020). *Development of Rotorcraft Forward Flight Analysis Code Using the Finite-State Dynamic Inflow Model*. PhD thesis, Master's thesis, University of California Davis.

Luo et al., 2015. Luo, J., Zhu, L., and Yan, G. (2015). Novel quadrotor forward-flight model based on wake interference. *AIAA Journal*, 53(12):3522–3533.

Misiorowski et al., 2019. Misiorowski, M., Gandhi, F., and Oberai, A. A. (2019). Computational study on rotor interactional effects for a quadcopter in edgewise flight. *AIAA Journal*, 57(12):5309–5319.

Moriarty and Hansen, 2005. Moriarty, P. J. and Hansen, A. C. (2005). Aerodyn theory manual. Technical report, National Renewable Energy Lab., Golden, CO (US).

Nguyen et al., 2018. Nguyen, D. H., Liu, Y., and Mori, K. (2018). Experimental study for aerodynamic performance of quadrotor helicopter. *Transactions of the Japan Society for Aeronautical and Space Sciences*, 61(1):29–39.

Peters and He, 1995. Peters, D. A. and He, C. J. (1995). Finite state induced flow models. ii-three-dimensional rotor disk. *Journal of Aircraft*, 32(2):323–333.

Romani et al., 2022. Romani, G., Grande, E., Avallone, F., Ragni, D., and Casalino, D. (2022). Computational study of flow incidence effects on the aeroacoustics of low blade-tip mach number propellers. *Aerospace Science and Technology*, 120:107275.

Roos, 1996. Roos, J. (1996). An analytical model for the determination of disc edge vortex strength, location and geometry at low to intermediate flying speeds.

Usov et al., 2022. Usov, D., Appleton, W., Filippone, A., and Bojdo, N. (2022). Low-order aerodynamic model for interference in multirotor systems. *Journal of Aircraft*, 59(6):1450–1462.

Yunus et al., 2025a. Yunus, F., Casalino, D., Romani, G., and Snellen, M. (2025a). Efficient prediction of propeller noise in non-axial uniform inflow conditions. *Aerospace Science and Technology*, 157:109860.

Yunus et al., 2025b. Yunus, F., Pavel, M. D., Romani, G., Casalino, D., and Snellen, M. (2025b). Modelling the disc edge vortices for propellers of multirotor evtol in forward flight. In *51th European Rotorcraft Forum, Venice (Italy)*.

Yunus et al., 2024. Yunus, F., von den Hoff, B., and Snellen, M. (2024). Predicting tonal noise of full-electric propeller-driven aircraft in outdoor environments using low-order models. In *30th aiaa/ceas aeroacoustics conference (2024)*, page 3418.

Zarri et al., 2022. Zarri, A., Dell'Erba, E., Munters, W., and Schram, C. (2022). Aeroacoustic installation effects in multirotorcraft: Numerical investigations of a small-size drone model. *Aerospace Science and Technology*, 128:107762.

Zawodny et al., 2023. Zawodny, N., Pettingill, N., and Thurman, C. (2023). Identification and reduction of interactional noise of a quadcopter in hover and forward flight conditions. In *INTER-NOISE and NOISE-CON Congress and Conference Proceedings*, volume 265, pages 2947–2958. Institute of Noise Control Engineering.